Journal of Power Sources 257 (2014) 325–334

Contents lists available at ScienceDirect

Journal of Power Sources

journal homepage: www.elsevier.com/locate/jpowsour

A holistic aging model for Li(NiMnCo)O_2 based 18650 lithium-ion batteries

Johannes Schmalstieg [a,c,*], Stefan Käbitz [a,c], Madeleine Ecker [a,c], Dirk Uwe Sauer [a,b,c]

[a] Electrochemical Energy Conversion and Storage Systems Group, Institute for Power Electronics and Electrical Drives (ISEA), RWTH Aachen University, Jägerstrasse 17/19, 52066 Aachen, Germany
[b] Institute for Power Generation and Storage Systems (PGS), E.ON ERC, RWTH Aachen University, Germany
[c] Jülich Aachen Research Alliance, JARA-Energy, Germany

HIGHLIGHTS

- Extended accelerated aging tests on lithium-ion batteries including storage and cycling.
- Detailed analysis of temperature and voltage dependencies of calendar cell aging.
- Detailed analysis of influence of cycle depth and SOC range on cycle aging.
- Lifetime prediction based on identified main aging phenomena.
- Comprehensive verification measurements for aging model.

ARTICLE INFO

Article history:
Received 5 December 2013
Received in revised form
21 January 2014
Accepted 4 February 2014
Available online 13 February 2014

Keywords:
Lithium-ion
Calendar aging
Cycle aging
Lifetime prognosis
Battery model

ABSTRACT

Knowledge on lithium-ion battery aging and lifetime estimation is a fundamental aspect for successful market introduction in high-priced goods like electric mobility. This paper illustrates the parameterization of a holistic aging model from accelerated aging tests. More than 60 cells of the same type are tested to analyze different impact factors. In calendar aging tests three temperatures and various SOC are applied to the batteries. For cycle aging tests especially different cycle depths and mean SOC are taken into account. Capacity loss and resistance increase are monitored as functions of time and charge throughput during the tests. From these data physical based functions are obtained, giving a mathematical description of aging. To calculate the stress factors like temperature or voltage, an impedance based electric-thermal model is coupled to the aging model. The model accepts power and current profiles as input, furthermore an ambient air temperature profile can be applied. Various drive cycles and battery management strategies can be tested and optimized using the lifetime prognosis of this tool. With the validation based on different realistic driving profiles and temperatures, a robust foundation is provided.

1. Introduction

Lithium-ion batteries are a key technology for current and future energy storage, whether they are used for mobile or stationary application. As the batteries' portion of cost is quite high for many applications, battery lifetime is a critical point for profitability. However, performing real life aging tests for every single application is an expensive and time consuming process which cannot be done in every case. Lifetime prediction using aging models can overcome this challenge as they have to be done only once per cell type.

Different approaches are used for modeling of lithium-ion batteries. The most realistic models are physico-chemical ones which simulate mostly single aging effects. However, these models are very slow and complex to parameterize. Therefore they are not suitable for aging prediction on a long time scale. In contrast neuronal network models have a very high computation speed, but they are usually not able to extrapolate aging for conditions that were not included in the learning set. Using physical based functions fitted to accelerated aging tests is a compromise between fast

* Corresponding author. Electrochemical Energy Conversion and Storage Systems Group, Institute for Power Electronics and Electrical Drives (ISEA), RWTH Aachen University, Jägerstrasse 17/19, 52066 Aachen, Germany. Tel.: +49 241 80 96911; fax: +49 241 80 92203.
E-mail address: jsc@isea.rwth-aachen.de (J. Schmalstieg).

http://dx.doi.org/10.1016/j.jpowsour.2014.02.012
0378-7753/

models on the one and realistic models on the other hand. These mathematical functions allow to reproduce the factors influencing aging, such as temperature or storage voltage, and extrapolating from a fixed set of tests to a wide range of applications.

For an aging prediction a lot of different aging factors have to be accounted. These factors are e.g. temperature, storage voltage and time for calendar aging and in addition cycle depth, SOC range, current rate and charge throughput for cycle aging [1,2]. Some studies have already published simulations dealing with a few of these factors, either calendar life [3–6] or cycle life [7]. Completely parameterized models including all of these factors and considering both calendar and cycle life are still missing.

This paper shows an accelerated aging test set including more than sixty cells of a commercial high-energy 18650 system with NMC cathode material. Both capacity loss as well as resistance increase are addressed. Calendar and cycle aging are considered separately. A holistic aging model including an impedance based electric-thermal model is presented. Finally the comparison between simulation results and verification measurements at nine different conditions will be shown.

2. Experimental

The tested battery was the Sanyo UR18650E, an 18650 round cell which is manufacturer rated with 2.05 Ah minimum and 2.15 Ah typically. The cathode active material is Li(NiMnCo)O_2 (NMC) and the anode consists of graphite. It is a high energy cell with a maximum discharge rate of 3C and 165 Wh kg^{-1} energy density. Voltage limits are 2.5 V for discharging and 4.2 V for charging with a proposed end of discharge voltage of 3.0 V and end of charge voltage of 4.1 V.

An OCV curve of the cell is shown in Fig. 1. A detailed analysis of the cell, the aging tests and the occurring processes can be found from Ecker et al. [8].

2.1. Calendar aging matrix

A list of all tested calendar aging test conditions can be found in Fig. 2. As the temperature dependency with an Arrhenius equation is already described by some authors [1,9], only three different temperatures are tested to verify this dependency. More attention was given to the voltage dependency, which is highly resolved with 10 different conditions. Each combination of temperature and voltage in the calendar aging test consists of three cells to get some statistics. All cells were held at a constant voltage (float conditions) during the tests. Every seven weeks a measurement of the cells capacity and inner resistance was performed.

2.2. Cycle aging matrix

The main focus of the cycle aging tests was the influence of cycle depth and mean SOC. A diagram with all cycle aging test conditions can be found in Fig. 3. All cycling tests were done at a current rate of 1C and a cell temperature of 35 °C. Temperature was logged using a sensor mounted on the surface of the cell. The mean SOC was set by a constant voltage charge using the OCV curve of the cell. Cycling was done Ah based around this point, with a reset of the mean SOC every 100 cycles. If a test had 0 or 100% SOC as limit, these points were used to set the cycle range. Checkups measuring the capacity and the inner resistance of the cell were made every 3 weeks.

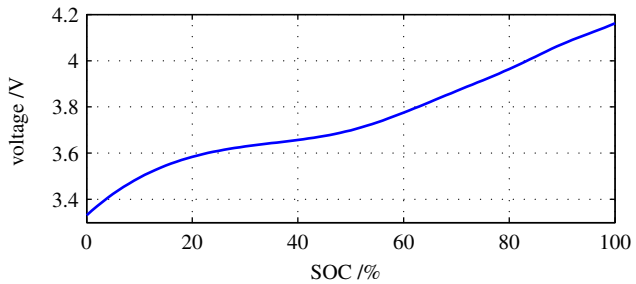

Fig. 1. OCV curve for a new cell (Sanyo UR18650E), measured at 35 °C.

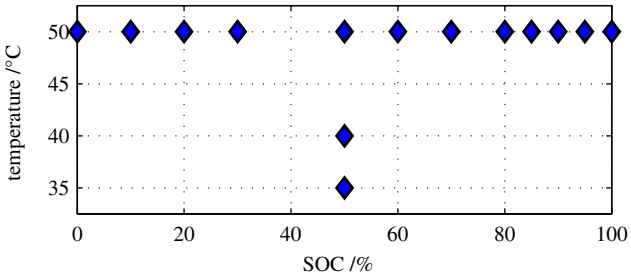

Fig. 2. Test matrix of calendar aging tests.

2.3. Checkups

All capacity and resistance measurements were done at 35 °C. The capacity measurement starts with a standard charge which is a 1C charge up to 4.2 V followed by a CV charge until current was below C/50. After that the capacity was measured during the 1C discharge down to 2.5 V. The inner resistance was measured at SOC steps of 10%, starting from 90% SOC down to 10% SOC. Every step was reached Ah based by discharging 1/10 of nominal capacity starting from a completely charged battery in the first step. At each step a pulse power characterization profile (PPCP) is applied to the battery.

The PPCP consists of an 18 s 2C discharge followed by a 40 s rest period. After that a 10 s 1C charge is applied, again followed by a 40 s rest period. A voltage response to this PPCP is shown in Fig. 4. From this profile various inner resistances are calculated, a 2, 10 and 17 s resistance for the discharge and a 2 and 10 s resistance for the charge. For the aging calculation the 10 s discharge resistance at 50% SOC is used. This resistance is calculated as the difference between the voltage before the discharge pulse and 10 s after the beginning of the discharge pulse divided by the current. All other resistances are calculated in a similar way.

3. Calendar aging

In the calendar aging tests, cells were stored at different temperatures and voltages. Each test condition was performed with 3

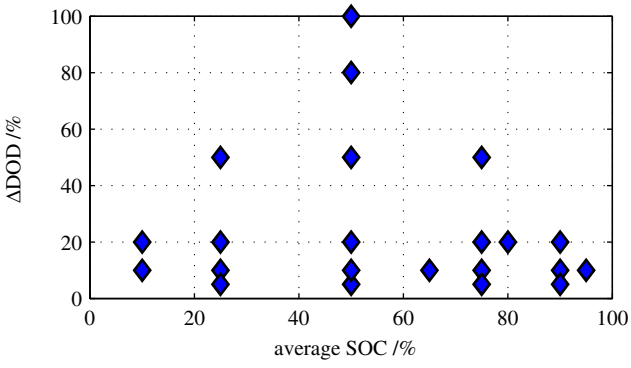

Fig. 3. Test matrix of cycle life tests performed on a 2.05 Ah cell. All cycle life tests were done at 1C and a cell temperature of 35 °C.

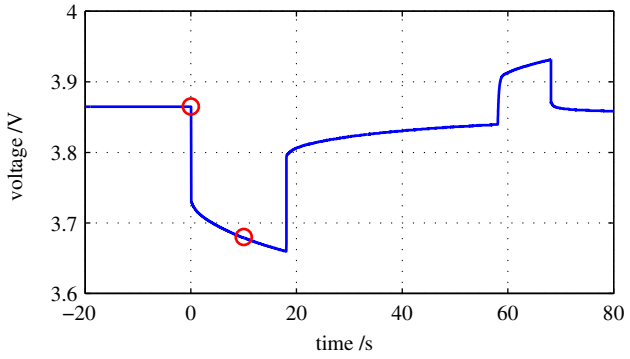

Fig. 4. Voltage reaction of a new cell to a PPCP. The two voltages used for calculating the 10 s discharge resistance are marked red. (For interpretation of the references to colour in this figure legend, the reader is referred to the web version of this article.)

cells to demonstrate the reproducibility of the experiment. The results show a very similar aging for cells tested under the same conditions, the measured capacities show an especially great uniformity [8].

Only the tests at 100% had a difference of more than 4% points between the best and worst cell. As these cells also had a very strong aging, they are excluded from further analysis. With a storage voltage of 4.162 V they were above the recommended end of charge voltage. This might lead to additional aging effect which cannot be scaled down to lower voltages.

For all tests a mean capacity loss and resistance increase has been calculated for every checkup. An error bar plot of both capacity and resistance in the 50 °C tests can be found in Fig. 5. The cells suffer increasing capacity loss and resistance increase with higher storage SOC and thereby higher voltage. Also the tests not displayed here with different temperatures show the expected increased aging with higher temperatures. A detailed discussion can be found in Ref. [8].

3.1. Fit method

To obtain a lifetime model out of the accelerated aging tests, a mathematical description of the aging processes is needed. The analysis was split into calendar and cycle aging. In the calendar aging tests, temperature and storage voltage were varied; a function should include these factors.

From Fig. 5 it can be seen, that different test conditions have unequal checkup numbers. This is due to the removal of cells which went below 75% of initial capacity or a later start after the first tests were done. For an aging function being directly fitted to all checkups this would have lead to variable impacts of different test conditions on the result. The influence of tests with moderate aging would have been overestimated while new started tests or tests with higher aging and therefore fewer checkups would have been underestimated.

To avoid this a two step fitting was done. In the first step, every single aging condition was fitted separately. For this, different fitting functions were tested. The best choice were functions, that had only one aging factor as fitting parameter. Afterward the dependency of this aging factor on temperature and voltage was analyzed.

3.2. Time dependency

For a cell with a carbon based anode, like the one used here, it is widely accepted in literature [10,11] that the dominant calendar aging effect is the formation of a so called solid electrolyte

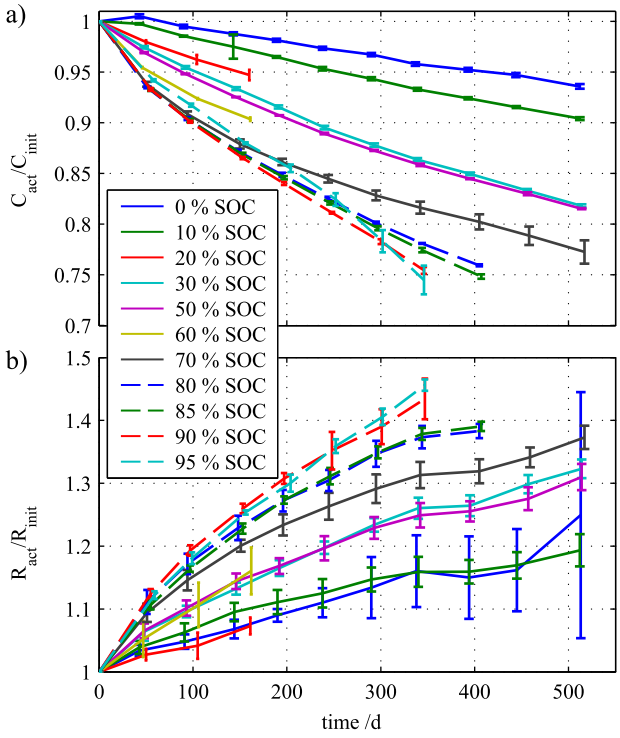

Fig. 5. a) Normalized capacity over time and b) normalized resistance over time for calendar aging tests at 50 °C. For each SOC the average on three cells under tests is shown. The capacities for cells under same conditions have a great uniformity, while resistance increase varies a bit.

interphase (SEI). The SEI is built up of decomposition products of the electrolyte, consuming lithium during formation and increasing resistance through the growing layer thickness [12]. Although there are different theories on SEI formation [13,14], both lead to a square root of time dependency. For some already published aging tests [9,13] this seems to be approved. Nevertheless the capacity decrease measured at this cell started with lower aging and seemed to have a share of linear aging which was also observed in Ref. [15]. Therefore a pure linear and a pure square root function are used together with a superposition of both and a function with $t^{0.75}$ as a medium function. The fits are done for both capacity C and resistance R, using n and α (or α_1 and α_2) as fitting variables.

$$C/R = n \mp \alpha \cdot t \tag{1}$$

$$C/R = n \mp \alpha \cdot \sqrt{t} \tag{2}$$

$$C/R = n \mp \alpha_1 \cdot t \mp \alpha_2 \cdot \sqrt{t} \tag{3}$$

$$C/R = n \mp \alpha \cdot t^{0.75} \tag{4}$$

For all fit functions the parameter n should be equal to 1 as all data is normalized to initial values. Anyway this parameter is set free for the fit to compensate deviations of the measured data. For further analysis only the aging factors α are used.

An example of the fit functions can be found in Fig. 6. The mean capacity of cells stored at 50 °C and 50% SOC is plotted together with the fit functions, showing a bad congruence of single linear (1) and square root functions (2). The superposed linear and square root function (3) and the function with $t^{0.75}$ (4) are similar and match the data well. The fit parameters for 50 °C and 50% can be found in Table 1 together with an average R^2 for all tests. In this

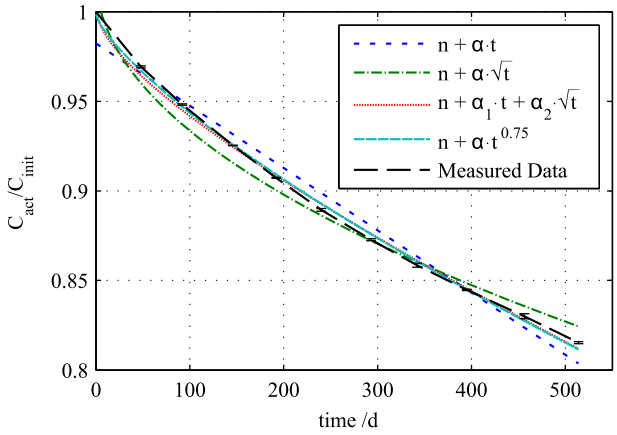

Fig. 6. Mean capacity for the cells stored at 50 °C and 50% SOC over time together with 4 different fit functions.

table and all following equations the fitting parameters are given without units. Instead the units of the input values are specified to allow recalculation. For Table 1 all times t has to be used in days.

Best results on the single tests were obtained using the superposed function (3), but the aging factors α_1 and α_2 do not have a clear trend over voltage (see Fig. 7). This might be due to scattering of the data which prohibits an exact division into linear and square root functions.

Therefore the function with $t^{0.75}$ is used for further analysis of the aging parameters. This function shows a similar shape in the required range and has only one aging factor which needs to be evaluated. The average R^2 value is not as good as the one from the superposed function, but better than the single linear or square root functions.

3.3. Voltage dependency

A plot of the aging factor over voltage for all tests performed at 50 °C both for resistance and capacity can be found in Fig. 8. The aging factor show a linear trend considering the whole voltage range. Therefore the function

$$\alpha_V(V) = a_1 \cdot V + a_2 \tag{5}$$

is chosen here to describe the dependency of aging factor α from voltage V, using the fitting parameters a_1 and a_2.

In contrast other papers found an exponential dependency [2] that is clearly not given here. Other work also done on these data sets [8] proposed a correlation between aging and graphite stages in the anode material, dividing the voltage dependency in single steps with nearly equal aging.

In this case for the aging model the small differences between a stepwise function and a simple linear dependency can be

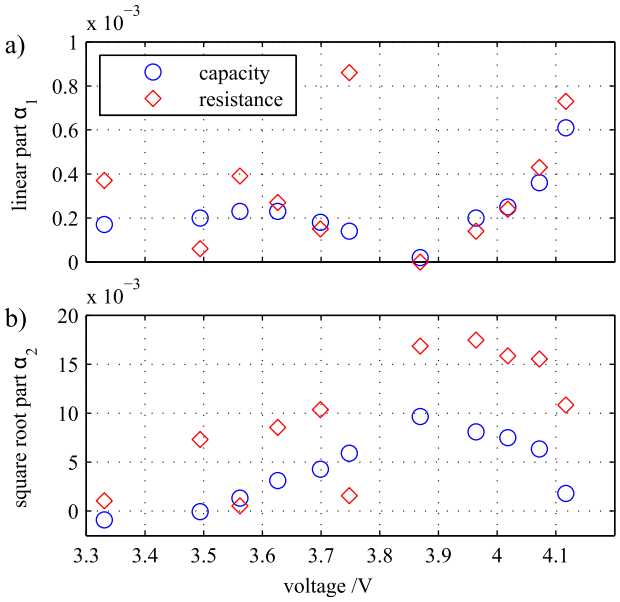

Fig. 7. Voltage dependency of the aging factors a) α_1 and b) α_2 over voltage from the superposed linear and square root function for tests performed at 50 °C.

neglected. For most applications voltage and SOC are changing during the simulated profile, sweeping over areas which underestimate or overestimate the aging. In total these effects should compensate over the full range. Therefore a linear regression was used to describe the voltage dependency in this model.

In the future a better knowledge on the aging behavior at different graphite stages could lead to a simplified parameterization of a stepwise defined function with a reduced number of needed tests.

3.4. Temperature dependency

For temperature dependency only three different temperatures were tested. A lot of literature already described the Arrhenius equation

$$\alpha_T(T) = a_1 \cdot \exp\left(-\frac{E_A}{RT}\right) \tag{6}$$

as a good matching function for temperature dependency. E_A is thereby the activation energy of a reaction happening at a temperature T, R is the gas constant. To test this equation with our data, a plot of $\ln(\alpha)$ over inverse temperature is shown in Fig. 9. The three temperatures were 35 °C, 40 °C and 50 °C. For both capacity and resistance the logarithm of aging factors give a linear dependency, confirming the applicability of the Arrhenius equation for these

Table 1
Fit parameter for capacity and resistance from the 50 °C and 50% SOC test. Four different fit functions with three to four free parameters were used. $\varnothing R^2$ is the mean R^2 value of all fitted tests. All fitting values are given without units, time values must be used in days.

	$n \mp \alpha \cdot t$		$n \mp \alpha \cdot \sqrt{t}$		$n \mp \alpha_1 \cdot t \mp \alpha_2 \cdot \sqrt{t}$		$n \mp \alpha \cdot t^{0.75}$	
	Capacity	Resistance	Capacity	Resistance	Capacity	Resistance	Capacity	Resistance
n	0.982	1.045	1.020	0.981	1.003	0.995	0.999	1.017
α	0.00035	0.00055	0.00862	0.01402			0.00173	0.00278
α_1					0.00018	0.00015		
α_2					0.00427	0.01037		
R^2	0.978	0.949	0.975	0.988	0.997	0.994	0.998	0.986
$\varnothing R^2$	0.974	0.952	0.960	0.965	0.997	0.987	0.989	0.978

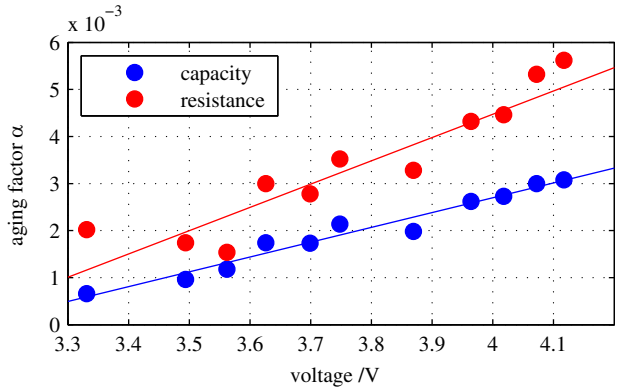

Fig. 8. Voltage dependency of the aging factor α over voltage from $C = n - \alpha \cdot t^{0.75}$ for tests performed at 50 °C together with a linear regression. Although the resistance has higher aging factors, capacity aging is restricting lifetime here as end of life is often defined as 20% of capacity loss or 100% resistance increase.

cells. Results of the linear interpolation are activation energies of 58.0 kJ mol^{-1} K^{-1} for the capacity and 49.8 kJ mol^{-1} K^{-1} for the resistance. Therefore a change from 20 to 30 °C accelerates calendar aging by a factor of 2.2 for capacity loss and 2.0 for resistance increase.

3.5. Fit function calendar aging

For a mathematical model of calendar aging the dependencies on voltage and temperature need to be combined. Here an aging factor α is used to describe the aging rate during a test of time t.

$$C = 1 - \alpha_{\text{cap}} \cdot t^{0.75} \tag{7}$$

$$R = 1 + \alpha_{\text{res}} \cdot t^{0.75} \tag{8}$$

The test at 50 °C and 50% SOC (3.699 V) is included both in voltage (α_V, see Eq. (5)) and temperature (α_T, see Eq. (6)) fit and therefore chosen as an intersection for both functions. As the two fitting functions do not exactly match at this point, the resulting mean value was calculated.

$$\alpha(50\,^\circ\text{C}, 3.699\,\text{V}) \stackrel{!}{=} \frac{\alpha_V(3.699\,\text{V}) + \alpha_T(50\,^\circ\text{C})}{2} = \alpha_{\text{Ø}} \tag{9}$$

Both functions were then scaled to match this mean value.

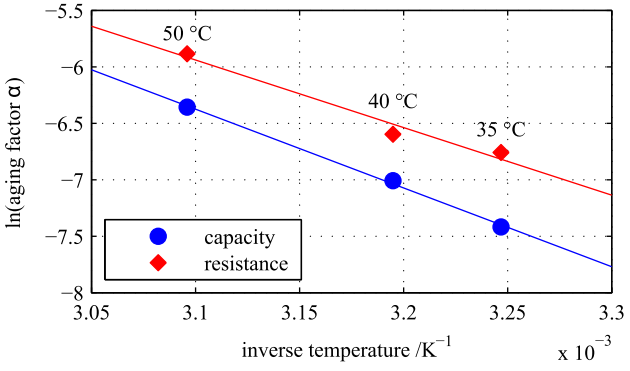

Fig. 9. Arrhenius plot of aging factor α for both capacity and resistance over inverse temperature. The shown temperatures are 35 °C, 40 °C and 50 °C. Also the linear regression for temperature dependency is shown.

$$\alpha_{T,\text{scaled}}(T) = \alpha_T(T) \cdot \frac{\alpha_{\text{Ø}}}{\alpha_T(50\,^\circ\text{C})} \tag{10}$$

$$\alpha_{V,\text{scaled}}(V) = \alpha_V(V) \cdot \frac{\alpha_{\text{Ø}}}{\alpha_V(3.699\,\text{V})} \tag{11}$$

The dependencies of the two single fits were combined and again scaled.

$$\alpha(T,V) = \frac{\alpha_{T,\text{scaled}}(T) \cdot \alpha_{V,\text{scaled}}(V)}{\alpha_{\text{Ø}}} \tag{12}$$

The resulting combined equation is

$$\alpha(T,V) = \frac{\alpha_V(V) \cdot \alpha_T(T) \cdot \alpha_{\text{Ø}}}{\alpha_V(3.699\,\text{V}) \cdot \alpha_T(50\,^\circ\text{C})}. \tag{13}$$

The combined aging factors for capacity and resistance are

$$\alpha_{\text{cap}}(T,V) = (7.543 \cdot V - 23.75) \cdot 10^6 \cdot e^{-\frac{6976}{T}} \tag{14}$$

$$\alpha_{\text{res}}(T,V) = (5.270 \cdot V - 16.32) \cdot 10^5 \cdot e^{-\frac{5986}{T}} \tag{15}$$

for tests done at a voltage V in volts and an absolute temperature T in kelvins. These equations allow one to calculate the calendar aging for arbitrary conditions of voltage and temperature. They are the basis for the cycle aging analysis in the next chapter.

4. Cycle aging

Cycling a battery leads to additional aging due to processes which do not occur during calendar aging. During intercalation and de-intercalation the material experiences a volume change which is a stress factor for the battery system. Results can be a crack-and-repair of the SEI which consumes lithium and increase the inner resistance or a contact loss of active material particles.

22 cycle aging tests varying cycle depth and average SOC were performed. All cycle aging tests were done at a temperature of 35 °C and a current of 1C. This would result in 12 equivalent full cycles per day, but real values are lower due to time for checkups and other unplanned rest periods.

During the time of cycling calendar aging also occurs. To get an analysis of the 'pure' cycle aging, all test data had to be adjusted by the calendar aging. The calendar capacity loss and resistance increase were calculated using the functions obtained from the tests discussed before and then added/subtracted from the measured capacities and resistances.

$$C_{\text{cyc}} = C_{\text{meas}} + \alpha_{\text{cap}}(V_{\text{meas}}, T_{\text{meas}}) \cdot t^{0.75} \tag{16}$$

$$R_{\text{cyc}} = R_{\text{meas}} - \alpha_{\text{res}}(V_{\text{meas}}, T_{\text{meas}}) \cdot t^{0.75} \tag{17}$$

To calculate the calendar aging of a cycle aging test, the voltage of the mean SOC was used together with the cycle test temperature of 35 °C. All discussion of cycle aging in this chapter refers to these adjusted values. A selection of typical 'pure' cycle aging curves can be found in Fig. 10.

Within literature sometimes a linear aging over charge throughput Q is found [16], but also work about square root aging was presented [7,17]. In our tests we found two different dependencies for capacity and resistance. For capacity loss a clear square root function can be found while the resistance increase is linear. This indicates that during cycling two different aging processes occur in the battery, one that has a strong impact on capacity and another that influences resistance.

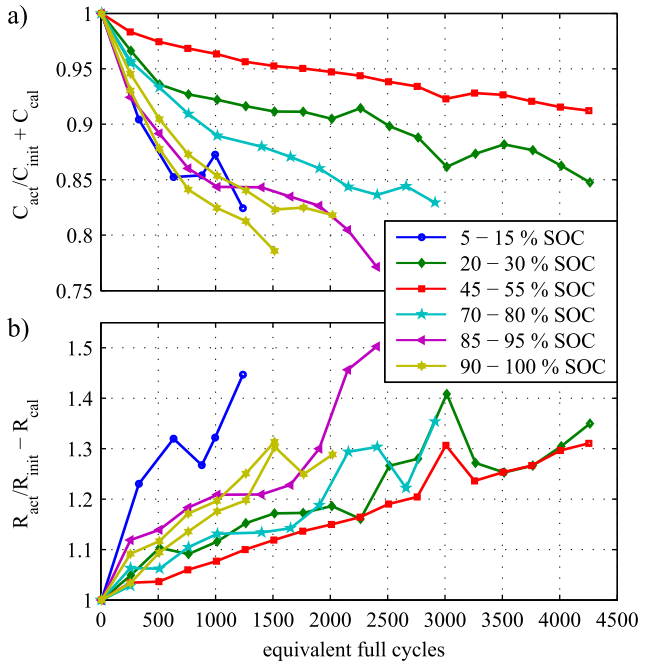

Fig. 10. a) Normalized capacity and b) normalized resistance over equivalent full cycles. Values are adjusted to the 'pure' cycle aging by subtracting the calculated calendar aging. The shown tests were done with 1C at 35 °C and a cycle depth of 10%. For the test 90–100% SOC two cells were tested.

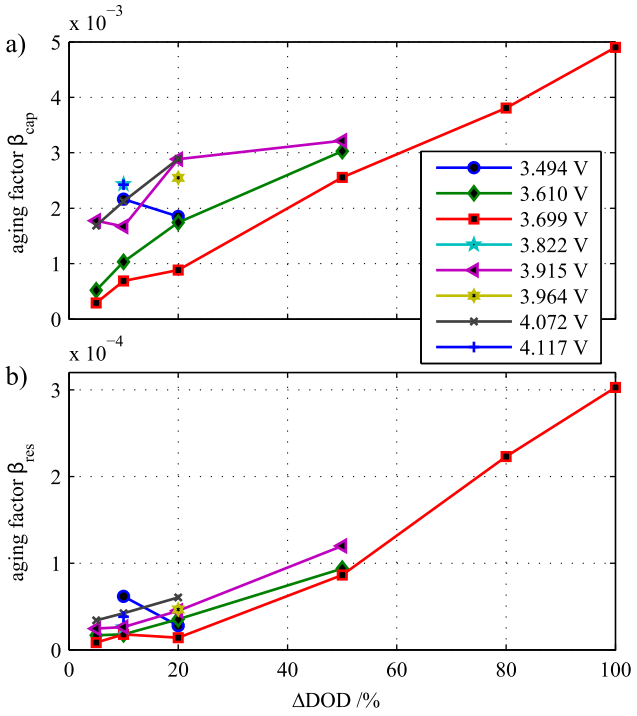

Fig. 11. a) Aging factor β_{cap} and b) aging factor β_{res} over cycle depth for different average voltages. All cycle tests were done with 1C at 35 °C.

$$C_{cyc} = 1 - \beta_{cap} \cdot \sqrt{Q} \tag{18}$$

$$R_{cyc} = 1 + \beta_{res} \cdot Q \tag{19}$$

Analysis was done with a two step fitting like before. In the first step, all single tests were fitted using Equations (18) and (19). After that the dependency of cycle aging factor β on cycle depth and average voltage were analyzed.

4.1. Dependency on cycle depth

Cycle depth is an important point to battery aging. For a lot of battery types and chemistries, deep cycles cause disproportional or exponential stronger aging compared to small cycle depths [18]. In these cases oversizing of battery capacity is an effective but also expensive option. With a good knowledge of cycle depth dependency, the oversizing can be reduced to a minimum.

Fig. 11 shows the aging factors β from the first step fits over cycle depth ΔDOD. Tests at equal average voltages are plotted in the same color. The plot indicates a non-exponential dependency, instead a more linear trend can be found. For capacity loss this linear dependency seems to be true for the full range while the resistance increase shows a constant minimal aging for low cycle depths.

4.2. Dependency on average voltage

Fig. 10 already indicates that cycling around a middle voltage leads to the lowest aging. Both for capacity loss as well as for resistance increase, the cycling between 45 and 55% SOC has the smallest effects. Cycling around lower or higher voltages increases the cycle aging rate.

A plot of all cycle aging factors β over average voltage is shown in Fig. 12. For all cycle depth a U-shaped function can be found with a minimum around 3.7 V average voltage.

For lifetime optimized charging strategies the dependency on average voltage has to be taken into account. From calendar aging aspects the lower SOC has advantages, but with cycling the optimum might shift to a SOC level around 50%.

4.3. Total fit function

With the aforementioned linear cycle depth (ΔDOD in the range of 0–1) and quadratic average voltage (ØV in Volt) dependency a fit was made to all aging factors β from the cycle aging tests. The resulting functions for cycling capacity loss and resistance increase are

$$\beta_{cap} = 7.348 \cdot 10^{-3} \cdot (ØV - 3.667)^2 + 7.600 \cdot 10^{-4} + 4.081 \cdot 10^{-3} \cdot \Delta DOD \tag{20}$$

and

$$\beta_{res} = 2.153 \cdot 10^{-4} \cdot (ØV - 3.725)^2 - 1.521 \cdot 10^{-5} + 2.798 \cdot 10^{-4} \cdot \Delta DOD \tag{21}$$

with all values of β_{res} below $1.5 \cdot 10^{-5}$ being set to this value to obtain a minimal aging as seen in Fig. 11.

The total aging function is then the superposition of calendar and cycle aging as shown in Equations (22) and (23). In this function the time t must be used in days and the charge throughput Q in ampere-hours. With this function a calculation of battery aging and lifetime is possible for all conditions.

$$C = 1 - \alpha_{cap} \cdot t^{0.75} - \beta_{cap} \cdot \sqrt{Q} \tag{22}$$

$$R = 1 + \alpha_{res} \cdot t^{0.75} + \beta_{res} \cdot Q \tag{23}$$

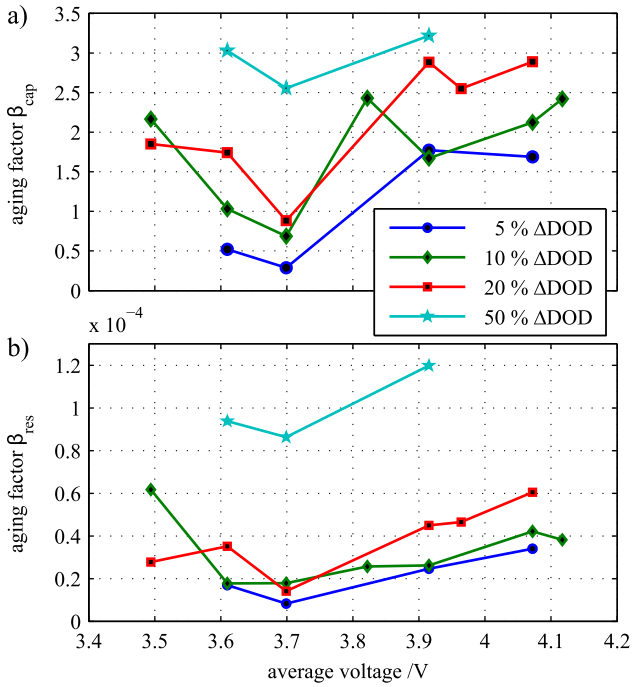

Fig. 12. a) Aging factor β_{cap} and b) aging factor β_{res} over average voltage for different cycle depths. The OCV at mean SOC of the cycling was chosen as average voltage. All cycle tests were done with 1C at 35 °C.

5. Model

To calculate lifetime and battery aging, the voltage and temperature of the battery are needed in each time step. Most applications only provide a current or power profile. Therefore a holistic model was built which consists of three parts:

- Impedance based electric model
- Thermal model
- Aging model.

These three model parts are called in a loop. A schematic of this integrated model is shown in Fig. 13. As the model is impedance based it does a fast computation and can easily be parameterized through electrochemical impedance spectroscopy (EIS) measurements [19,20]. The aging model is based on the equations developed from the accelerated aging tests. Every aging parameter was analyzed separately and put into a mathematical equation, therefore the effects can be extrapolated to ranges that have not been tested (e.g. lower temperatures).

The model takes a load profile (can be power or current) as input. Furthermore a profile for ambient air temperature can be included, else a constant temperature is chosen.

The impedance based electrical model uses an equivalent electric network that consists of a series resistance, two ZARC elements and an OCV source. The network can be found in Fig. 14. The single elements are parameterized using lookup tables for different temperatures and SOC obtained from fitted EIS measurements. The model simulates the voltage and SOC for any given load profile.

A thermal model is coupled to the electric model. Heat production is based on ohmic losses calculated by the electric model. Heat transfer to the ambient air is modeled as heat conductivity with variable factor to match different mounting scenarios.

Voltage, temperature, SOC and current are taken from the combined electric-thermal model as inputs for the aging model.

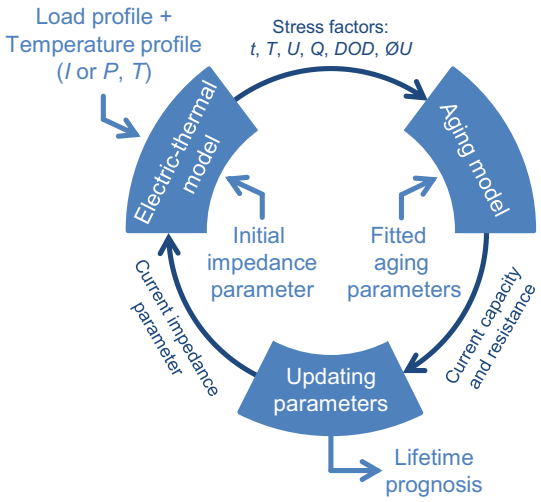

Fig. 13. Graphical representation of the holistic model. Calculation is done in a loop with load profile, impedance parameters and aging factors as input. Output is the remaining capacity and resistance together with a lifetime estimation.

From this data cycle depth and average SOC are calculated. The average voltage for cycle aging is only calculated during current flow, rest periods do not influence it. Calendar and cycle life aging is calculated separately for every single time step using the aging functions gained from the accelerated aging tests. To get the total aging, calendar and cycle aging are added.

The impedance parameters are then updated. All capacitances from the equivalent electric network are scaled like the normalized capacity and all resistances are scaled like the normalized resistance. After that a new loop is started with the aged parameters. A schematic of the aging calculation is given in Fig. 15.

6. Verification

Along with the accelerated aging tests a verification profile has been applied to the batteries. For this verification profile a driving cycle was used together with charge and rest periods. The driving profile was taken from real car measurements done in Aachen, including city and highway driving. The power was scaled down to meet the specification of the battery. An overview on the driving part of the profiles can be found in Fig. 16, the power together with the SOC and voltage for a new cell are shown.

Three different test profiles were built with this load profile. Plots are displayed in Fig. 17.

The first and second profile consist of two driving parts a day separated with long rest periods. The first profile has the charge periods just after the driving part while the second one charges before driving. The third profile is an alternation of driving and charging without long rest periods. The charging in all three profiles is performed with 1C.

The profiles tests were performed with monthly changing ambient air temperature. The temperatures are average values for Germany from 2001 to 2010 [21]. A diagram of the temperatures is shown in Fig. 18. The initial month for the verification was September.

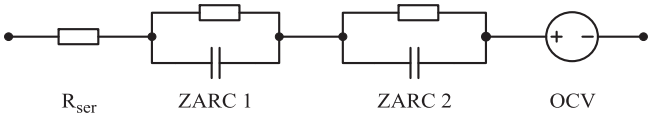

Fig. 14. Equivalent electric network used in the impedance based model.

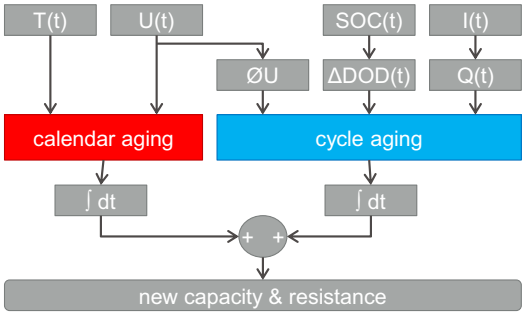

Fig. 15. Schematic of the calculation process within the aging model. Input values are given for every single time step, calendar and cycle life aging are integrated on these single aging steps.

Temperatures inside a battery pack build in a car might be higher than the ambient air temperature. Therefore higher temperatures have also been tested. Tests with all three profiles have also been performed at the average temperatures plus 10 °C and at plus 20 °C.

Checkups on these cells have been done every month with the same method like the other cycle life tests described in Chapter 2.3.

The measured data for both capacity loss and resistance increase for the verification profiles can be found in Fig. 19 together with the simulation results.

The figure shows that the aging predicted by the model matches the measurements well for capacity loss although the model was only parameterized at temperatures much higher than the temperatures applied in the verification profile. The extrapolation using the Arrhenius Equation (6) seems to be valid down to temperatures at 0 °C. Also the assumption that there is no or only a small temperature dependency for the cycle aging proves true in this verification.

In comparison the results for profile 1 and profile 2 are similar which is surprising as they have completely different charging strategies. These strategies lead to different average voltages during the rest period. For a new cell it is 4.174 V for profile 1 versus 3.970 V for profile 2, both at +0 °C. Using function (14) this is a factor of 1.25 in calendar aging between the two strategies. But as calendar aging

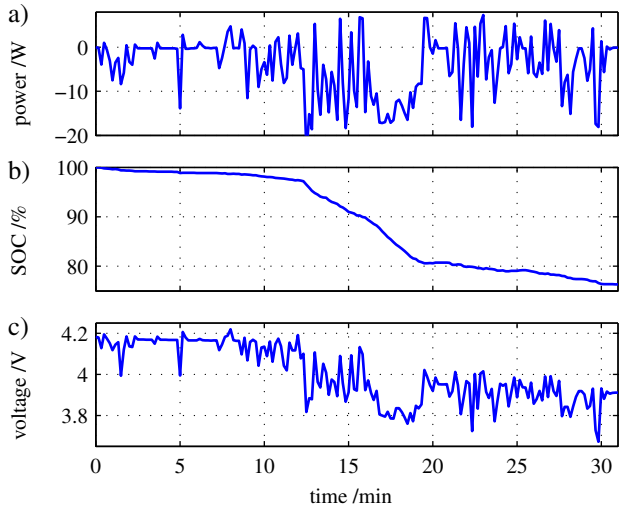

Fig. 16. a) Driving part of the power profile. b) SOC and c) voltage plot for this profile and a new cell. All values are plotted over time. The profile is taken from real car measurements, including city and highway driving.

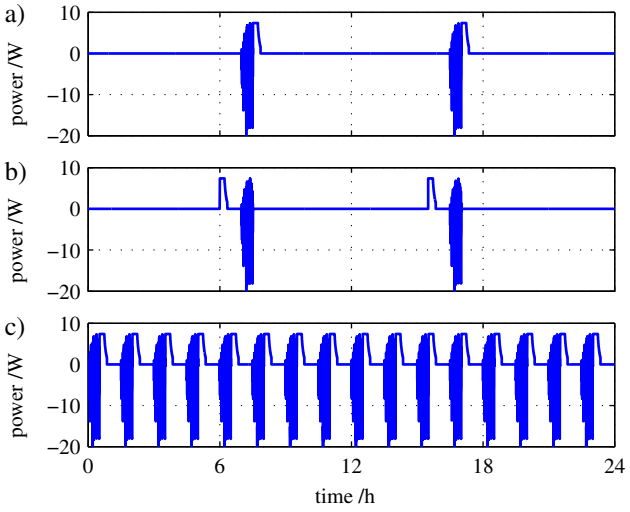

Fig. 17. Three power profiles over time for model evaluation. All are based on the driving cycle shown in Fig. 16. a) Charge after driving, b) charge before driving and c) no rest periods.

is much smaller than cycle aging for most temperatures the influence on total aging is low and both strategies look similar.

The simulated resistances for most verification profiles are lower than the measured ones. The biggest relative deviation is found in cases where the simulated resistance increase is very small, for higher aging rates measurement and simulation match better.

As this cell shows only a small resistance increase in comparison with the capacity loss, the last one will limit the lifetime for nearly all application. Therefore the correct capacity prediction is more valuable than the resistance simulation.

The reason for the deviation in resistance increase might be high currents used in the driving profile. While all accelerated aging tests were done at 1C the verification profile had currents up to 3C for discharging. This might increase internal stress on the particles. Beside the filming reaction which is included in the aging model, a second effect seems to occur which increases the resistance without consuming lithium. Due to the high currents there is a fast volume change during intercalation and de-intercalation. A possible explanation for this second effect could be partial loss of interparticle contact during the volume change.

7. Conclusion

In this work an aging model for an 18650 cell with NMC cathode chemistry was established. An extensive set of both calendar and cycle aging tests has been performed including more than 60 cells.

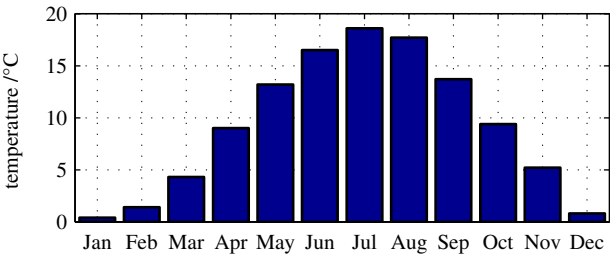

Fig. 18. Temperatures used for model verification. For each month an ambient temperature is given to the simulation. Values are average temperatures for Germany from 2001–2010 [21].

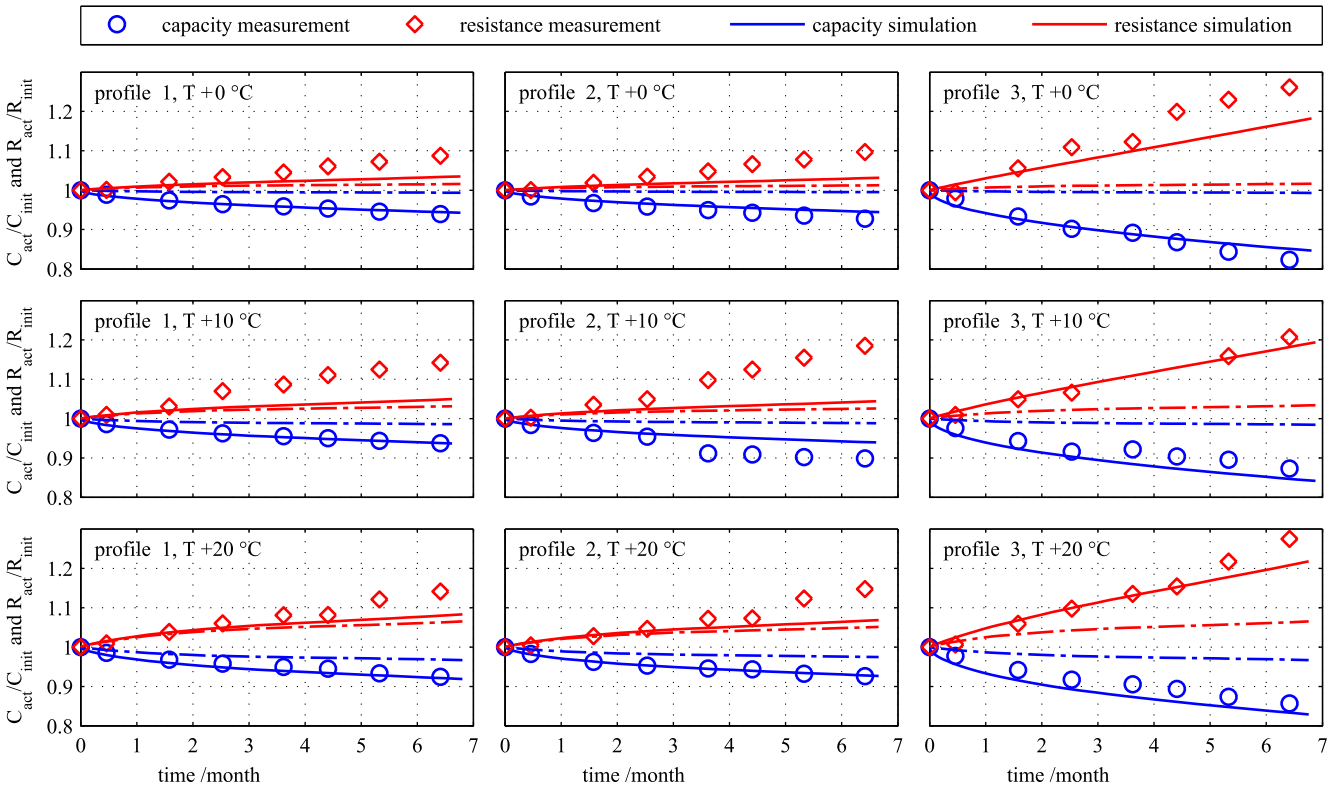

Fig. 19. Comparison between measured data (circles) and simulation results (lines). The dashed lines show the calendar part of the aging. Three profiles were tested at three temperature levels. Both capacity and resistance are shown for each test.

Varied parameters were voltage/SOC and temperature for the calendar tests. In the cycle aging tests cycle depths and average voltage were studied. During all tests checkups with actual capacity and inner resistance were determined.

Using these values for capacity fade and resistance increase mathematical functions have been fitted. For both calendar and cycle aging tests a two step fitting was done. The resulting fitting functions include the dependency of capacity and resistance on time respectively charge throughput and the other varied parameters.

For the tested cell the calendar aging could not be modeled using a square root function of time. The data indicated the occurrence of a second main aging effect besides normal SEI growth which has a linear time dependency. As both effects could not be separated by the fit a $t^{0.75}$ dependency was used. For temperature dependency the Arrhenius equation was used. On this cell the aging speed increased linearly with voltage for a calendar aging test.

The cycle aging data was adjusted by the calendar aging prediction. Fits were done with two different functions for capacity loss and resistance increase. The capacity was implemented using a square root function of charge throughput while the resistance had a linear dependency. Both capacity and resistance had the lowest aging while cycling around 3.7 V (50% SOC), lower or higher cycle ranges increased aging. The effect of cycle depth on aging was linear.

The fit functions were implemented in an aging model which was coupled to an impedance based electric-thermal model. Three different verification profiles were tested on the cells, each at three temperature levels. In all nine cases the predicted capacity loss matched the measured data. For low resistance increase the model underestimated the aging, for higher resistance increase the congruence is quite good.

This holistic model is able to predict the aging for different drive cycles and management strategies. It can be used with current and power profiles as input, also ambient air temperature profiles changing over the seasons can be included. The model is a powerful tool to optimize BMS strategies and lifetime for all applications using this cell.

Acknowledgment

The project upon which this publication is based was funded by the Federal Ministry of Education and Research under project numbers 03X4613D (Li-Five) and 13N10656 (e performance) as well as by the Impuls- und Vernetzungsfond der Helmholtz-Gemeinschaft e.V. through the framework of the research initiative HGF Energie Allianz. The authors of this publication are responsible for its content.

References

[1] S. Käbitz, J.B. Gerschler, M. Ecker, Y. Yurdagel, B. Emmermacher, D. André, T. Mitsch, D.U. Sauer, J. Power Sources 239 (2013) 572–583, http://dx.doi.org/10.1016/j.jpowsour.2013.03.045.
[2] M. Ecker, J.B. Gerschler, J. Vogel, S. Käbitz, F. Hust, P. Dechent, D.U. Sauer, J. Power Sources 215 (2012) 248–257, http://dx.doi.org/10.1016/j.jpowsour.2012.05.012.
[3] E. Thomas, I. Bloom, J. Christophersen, V. Battaglia, J. Power Sources 184 (1) (2008) 312–317, http://dx.doi.org/10.1016/j.jpowsour.2008.06.017.
[4] E. Thomas, I. Bloom, J. Christophersen, V. Battaglia, J. Power Sources 206 (2012) 378–382, http://dx.doi.org/10.1016/j.jpowsour.2012.01.106.
[5] B.Y. Liaw, R.G. Jungst, G. Nagasubramanian, H.L. Case, D.H. Doughty, J. Power Sources 140 (1) (2005) 157–161, http://dx.doi.org/10.1016/j.jpowsour.2004.08.017.
[6] M. Safari, M. Morcrette, A. Teyssot, C. Delacourt, J. Electrochem. Soc. 156 (3) (2009) A145–A153, http://dx.doi.org/10.1149/1.3043429.
[7] J. Wang, P. Liu, J. Hicks-Garner, E. Sherman, S. Soukiazian, M. Verbrugge, H. Tataria, J. Musser, P. Finamore, J. Power Sources 196 (8) (2011) 3942–3948, http://dx.doi.org/10.1016/j.jpowsour.2010.11.134.
[8] M. Ecker, N. Nieto, S. Käbitz, J. Schmalstieg, H. Blanke, A. Warnecke, D.U. Sauer, J. Power Sources 248 (2014) 839–851, http://dx.doi.org/10.1016/j.jpowsour.2013.09.143.

[9] I. Bloom, S.A. Jones, E.G. Polzin, V.S. Battaglia, G.L. Henriksen, C.G. Motloch, R.B. Wright, R.G. Jungst, H.L. Case, D.H. Doughty, J. Power Sources 111 (1) (2002) 152–159, http://dx.doi.org/10.1016/S0378-7753(02)00302-6.
[10] M. Broussely, P. Biensan, F. Bonhomme, P. Blanchard, S. Herreyre, K. Nechev, R. Staniewicz, J. Power Sources 146 (1–2) (2005) 90–96, http://dx.doi.org/10.1016/j.jpowsour.2005.03.172.
[11] J. Vetter, P. Novák, M. Wagner, C. Veit, K.-C. Möller, J. Besenhard, M. Winter, M. Wohlfahrt-Mehrens, C. Vogler, A. Hammouche, J. Power Sources 147 (1–2) (2005) 269–281, http://dx.doi.org/10.1016/j.jpowsour.2005.01.006.
[12] E. Peled, J. Electrochem. Soc. 126 (12) (1979) 2047–2051, http://dx.doi.org/10.1149/1.2128859.
[13] M. Broussely, S. Herreyre, P. Biensan, P. Kasztejna, K. Nechev, R. Staniewicz, J. Power Sources 97–98 (2001) 13–21, http://dx.doi.org/10.1016/S0378-7753(01)00722-4.
[14] H.J. Ploehn, P. Ramadass, R.E. White, J. Electrochem. Soc. 151 (3) (2004) A456–A462, http://dx.doi.org/10.1149/1.1644601.
[15] J. Belt, V. Utgikar, I. Bloom, J. Power Sources 196 (23) (2011) 10213–10221, http://dx.doi.org/10.1016/j.jpowsour.2011.08.067.
[16] K. Takei, K. Kumai, Y. Kobayashi, H. Miyashiro, N. Terada, T. Iwahori, T. Tanaka, J. Power Sources 97–98 (2001) 697–701, http://dx.doi.org/10.1016/S0378-7753(01)00646-2.
[17] R. Wright, J. Christophersen, C. Motloch, J. Belt, C. Ho, V. Battaglia, J. Barnes, T. Duong, R. Sutula, J. Power Sources 119–121 (2003) 865–869, http://dx.doi.org/10.1016/S0378-7753(03)00190-3.
[18] D.U. Sauer, in: J. Garche (Ed.), Encyclopedia of Electrochemical Power Sources, Elsevier, Amsterdam, 2009, pp. 805–815, http://dx.doi.org/10.1016/B978-044452745-5.00137-4.
[19] P. Mauracher, E. Karden, J. Power Sources 67 (1–2) (1997) 69–84, http://dx.doi.org/10.1016/S0378-7753(97)02498-1.
[20] S. Buller, M. Thele, R. De Doncker, E. Karden, IEEE Trans. Ind. Appl. 41 (3) (2005) 742–747, http://dx.doi.org/10.1109/TIA.2005.847280.
[21] Deutscher Wetterdienst, Zeitreihen von Gebietsmitteln, July 2013. http://www.dwd.de/bvbw/appmanager/bvbw/dwdwwwDesktop?_nfpb=true&gsbSearchDocId=809418.